colloids and interfaces

MDPI

Article

Hydrophobic Forces Are Relevant to Bacteria-Nanoparticle Interactions: *Pseudomonas putida* Capture Efficiency by Using Arginine, Cysteine or Oxalate Wrapped Magnetic Nanoparticles

Federico Figueredo [1], Albert Saavedra [1], Eduardo Cortón [1,*] and Virginia E. Diz [2,*]

[1] Laboratory of Biosensors and Bioanalysis (LABB), Biochemistry Department, IQUIBICEN-CONICET, FCEN, UBA, Buenos Aires 1428, Argentina; figueredofederico@yahoo.com (F.F.); albert.saavedra.olaya@gmail.com (A.S.)

[2] Departamento de Química Inorgánica, Analítica y Química Física, FCEN, UBA, Buenos Aires 1428, Argentina

* Correspondence: eduardo@qb.fcen.uba.ar (E.C.); dizvirginia@gmail.com (V.E.D.); Tel.: +54-11-4576-3342 (E.C.)

Received: 23 May 2018; Accepted: 15 July 2018; Published: 18 July 2018

Abstract: Size, shape and surface characteristics strongly affect interfacial interactions, as the presented among iron oxide nanoparticles (NPs) aqueous colloids and bacteria. In other to find the forces among this interaction, we compare three types of surface modified NPs (exposing oxalate, arginine or cysteine residues), based on a simple synthesis and derivation procedure, that allows us to obtain very similar NPs (size and shape of the magnetic core). In this way, we assure that the main difference in the synthesized NPs are the oxalate or amino acid residue exposed, an ideal situation to compare their bacterial capture performance, and so too the interactions among them. Field emission scanning electron microscopy showed homogeneous distribution of particle sizes for all systems synthesized, close to 10 nm. Magnetization, zeta potential, Fourier transformed infrared spectrometry and other studies allow us further characterization. Capture experiments of *Pseudomonas putida* bacterial strain showed a high level of efficiency, independently of the amino acid used to wrap the NP, when compared with oxalate. We show that bacterial capture efficiency cannot be related mostly to the bacterial and NP superficial charge relationship (as determined by z potential), but instead capture can be correlated with hydrophobic and hydrophilic forces among them.

Keywords: amino acid; bacteria; FT-IR spectra; magnetite; *Pseudomonas putida*; interfacial interactions; synthesis

1. Introduction

Superparamagnetic, small size and low toxicity nanoparticles (NPs) of magnetite (Fe_3O_4) are very versatile systems with multiple applications in science and technology [1]. Some of them were reviewed recently and include magnetic storage media [2], biosensing applications [3], medical applications such as targeted drug delivery [4], contrast agents in magnetic resonance imaging [5,6] and magnetic inks for ink-jet printing [7].

The co-precipitation technique is probably the simplest and most efficient chemical pathway to obtain magnetic NPs. Iron oxides are usually prepared by aging a stoichiometric mixture of ferrous and ferric salts in aqueous media. The chemical reaction of Fe_3O_4 formation may be described as: $Fe^{2+} + 2Fe^{3+} + 8OH^- = Fe_3O_4 + 4H_2O$. According to the thermodynamics of this reaction, complete precipitation of Fe_3O_4 should be expected at a pH between 8 and 14 in an oxygen-free environment.

However, magnetite is sensitive to oxidation and then transformed into magnemite (γFe_2O_3) in the presence of oxygen. Bubbling nitrogen gas through the solution not only protects against critical oxidation of the magnetite, but also reduces the particle size when compared to methods without oxygen removal [8,9]. The size and shape of the NPs can be also tailored by adjusting other variables such as pH, ionic strength, temperature, nature of the salts (chlorides, sulfates or perchlorates), or the ferrous/ferric ions concentration ratio [10,11]. For example, particle size will be low if the ionic strength of the medium and pH is high, since these two parameters determine the chemical composition of the crystal surface and the electrostatic surface charge of the NPs [12]. The control of the monodisperse size distribution is very important since the properties of the nano-crystals strongly depend upon the dimension of the NPs.

One of the most complicated problems is the NP aggregation. If this happens, surface area decreases, making them less efficient for absorbing either inorganic or organic compounds. Moreover, some applications rely on the strong interactions of living cells, as bacteria, with surface modified NPs. The stability of a magnetic colloidal suspension results from the equilibrium between attractive and repulsive forces [13]. In fact, it depends on different types of interactions: van der Waals forces, electrostatic repulsive forces, magnetic dipolar forces and steric repulsion forces [14]. One possible way to overcome the aggregation problem is the addition of stabilizing agents during the formation of magnetite, as organic anions (carboxylates, α hydroxyl carboxylate ions or oleic acids), polymers (dextran, carboxydextran or polyvinyl alcohol), surfactant molecules or inorganic species that minimize the attractions between the NPs [15]. Functional groups, including carboxylates, phosphates and sulfates, are known to bind the surface of magnetites [16]. When these molecules are used for the synthesis of magnetite, according to the molar ratio between the organic ion and the iron salts, the chelation of these organic ions on the iron oxide surface can either prevent nucleation, producing larger particles or inhibit the growth of the crystal nucleus, leading to small NPs [17]. As a result, new functional groups appear at the surface of the magnetic NPs, so the choice of the stabilizer is also determined by the intended final use. This is especially important for many applications on real samples, in which physical-chemical conditions (as pH, redox potential, ionic strength, among other) could impair the NP performance.

Surface modification of magnetic NPs with small organic molecules such as amino acids present many advantages as low cost, good biocompatibility and different available functional groups and organic residues. Amino acids are produced by simple industrial processes at low cost, are considered low toxicity molecules, and contain at least carboxyl and amino functional groups. In addition, many of them contain other functional groups such as sulfur, guanide, thiol and phenolic hydroxyl groups. All of these functional groups could be also covalently attached to other biocompatible molecules as DNA, antibodies, proteins, among others. In the last few years, surface modification of magnetic NPs with amino acids were reported for various applications on the field of magnetic resonance imaging, drug delivery, immunoassays and magnetic separation processes [18]. There are 20 natural amino acids with different isoelectric points, and a group of them have been proposed as stabilizers for various applications due to their charged side chains which have a good potential to bind anions, cations, organic molecules or cells through intermolecular forces over a wide pH range.

Cell interaction with solid materials can be related to relatively specific or unspecific relations; the first group has been studied more, and are related to molecules designed for molecular recognition that can target or attach to specific parts of the microorganisms, as antibodies, aptamers or lectins, among others [19]. However, generic non-specific interactions among NPs and microbial cells are more difficult to understand, mainly due to the complexity and variability of the external or exposed parts of the microorganisms, which include bacteria cellular membranes and cellular wall, and the possibility of active or passive NP internalization. Some aspects among NP size, shape, and charge, among others, have been previously reviewed [20].

The possibility to have a non-specific attraction between bacteria and magnetic NPs represents a technological advantage for total bacteria capture, in contrast to antibody modified NPs, which have

affinity just for a defined chemical group of single type or group of bacteria. The presented study shows a simple and easy synthesis procedure for the functionalization of magnetic NPs. We demonstrate by using two very different amino acids (a basic and a sulfur containing amino acids, arginine and cysteine, respectively) that the interaction with a model bacteria is mostly independent of the amino acid exposed. The comparison among amino acid and oxalate modified NPs at different pHs show the relevance of hydrophobic interactions between the bacteria and the NPs to explain the high bacterial capture efficiency of the NPs used here.

There are several technological ways to separate microorganisms from a solution; each method depends on several factors or requirements. Some relevant factors are the volume to be treated, cost, microbial viability and posterior use of the concentrated cells, if any. For example, filtration and centrifugation can be an effective method for small and medium volumes, but not for very large volumes, as needed for tap water production, where bacteria is eliminated by using aggressive substances, as chlorine, chloramines, and/or ozone. As bacteria develop resistance to different substances, and some of those products and by-products are toxic to humans, the development of new bacteria decontamination strategies of great urgency and importance are needed, as the use NPs [21]. Moreover, NPs that capture most of the bacteria present in complex matrices, as food and clinical samples, can be of great use to improve methods devoted to protect consumers, diagnosis and to treat infectious diseases. As an interesting example, Abejonar et al. show [22] an interesting method to destroy persistent microbial biofilms that lead to chronic infections. After magnetic NPs interact with *Staphylococcus aureus* biofilms, heat is induced by magnetic field stimulation (magnetic hyperthermia) helping to destroy the bacteria and biofilm, otherwise resistant to antibiotic treatment.

In this paper, magnetite NPs of ca. 10 ± 2 nm of diameter were functionalized with arginine (Fe_3O_4@Arg) and cysteine (Fe_3O_4@Cys). During the synthesis, oxalate ions may be adsorbed first on the surface of the magnetite NPs by coordinating via one or two of the carboxylate functionalities, depending upon steric necessity and the curvature of the surface. These leaves at least one carboxylic acid group exposed to the solvent, making the surface negatively charged and hydrophilic [23]. The functionalization process involves the substitution of oxalate stabilized on the surface of NPs with arginine and cysteine amino acids. The amino acid functionalization was confirmed by a Fourier transform infrared (FT-IR) spectroscopy technique, energy dispersive spectroscopy (EDS) and zeta potential. We also show the performance of the synthesized NP to capture efficiently bacteria from water. In this case, the presence of a biological molecule over the NPs surface could enhance the interaction between NPs and the bacterial cell membrane by van der Waals, hydrophobic or electrostatic forces among others.

2. Materials and Methods

2.1. Reagents and Microbial Culture

Iron (III) chloride hexahydrate ($FeCl_3 \cdot 6H_2O$), iron (II) sulphate heptahydrate ($FeSO_4 \cdot 7H_2O$), ammonium hydroxide solution (NH_4OH), ammonium oxalate ($(NH_4)_2C_2O_4$) and sodium hydroxide (NaOH) were all of analytical grade. L-arginine hydrochloric acid and L-cysteine hydrochloric acid were obtained from Sigma-Aldrich (St. Louis, MO, USA). *Pseudomonas putida* KT2440 was kindly provided by Dr. S. Ruzal (Universidad de Buenos Aires, Buenos Aires, Argentina).

2.2. Synthesis of Oxalate Coated Fe_3O_4 NPs (Fe_3O_4@Oxa)

The synthesis of Fe_3O_4@Oxa NPs was performed following the procedure reported by Tie et al. [24], but with some changes described below. In a typical synthesis, 6.22 g of $FeCl_3 \cdot 6H_2O$ (23 mmoles of Fe^{3+}) and 3.16 g of $FeSO_4 \cdot 7H_2O$ (11.3 mmoles of Fe^{2+}) were added to 100 mL of double distilled water bubbled under a nitrogen atmosphere and maintained at 70 °C with magnetic agitation. After 30 min, 10 mL of ammonium hydroxide (NH_4OH) concentrated and 0.15 g of ammonium oxalate (12 mmoles of $C_2O_4^{2-}$) were incorporated into the solution. After 1.5 h at 70 °C under a nitrogen

atmosphere, a black precipitate was separated using a neodymium magnet and then washed three times with deoxygenated double distilled water. Samples were dried in vacuum at 25 °C for four days. In this synthesis, we used a molar ratio of Fe^{3+}:Fe^{2+}:$C_2O_4^{2-}$ equal to 2:1:1 instead of the 2:1:0.1 molar ratio proposed previously [24].

2.3. Synthesis of Amino Acids Coated Fe_3O_4 NPs from Fe_3O_4@Oxa

In addition, 0.5 g of Fe_3O_4@Oxa was suspended in 150 mL of deoxygenated double distilled water adjusted to pH 5, under a nitrogen atmosphere. Then, 3.66 g of L-arginine or 2.55 g of L-cysteine (21 mmoles of each one) were added. The mixture was agitated in an orbital shaker at 30 °C for 4 h. A black precipitate was obtained and washed in a similar way previously described (using a magnet). In all cases, pH values were adjusted with NaOH or HCl. This process involves exchanging oxalate by L-cysteine or L-arginine in the surface of the NPs (Figure 1).

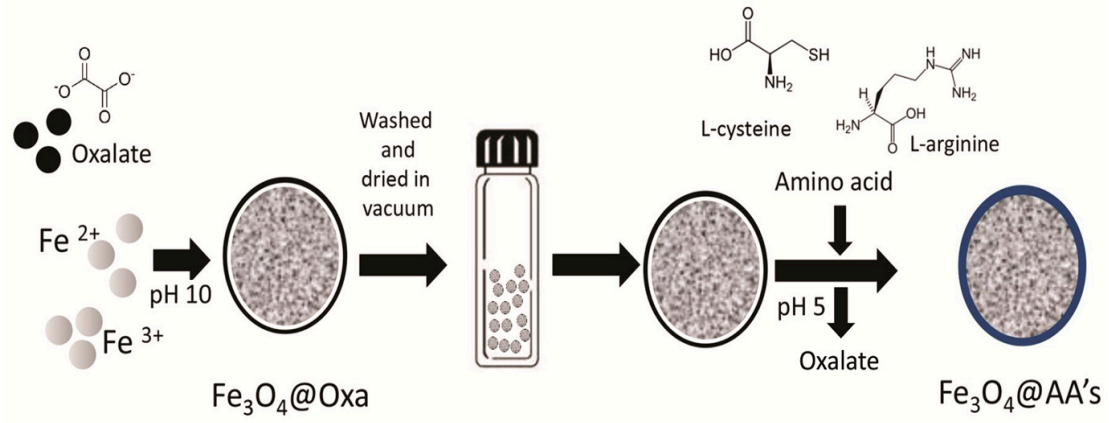

Figure 1. Schematic procedure applied to synthesize amino acid (AA) coated Fe_3O_4 nanoparticles (NPs). Depending on the AA used in the substitution, one or another type of AA modified NPs were obtained (F_3O_4@AA's).

2.4. Characterization Methods

Field emission scanning electron microscopy (FESEM) images were obtained with general-purpose high-resolution equipment (Carl Zeiss AG, Supra 40, Oberkochen, Germany). Zeta potential measurements were determined with a Zetasizer Nano ZS (Malvern Instruments Ltd., Malvern, UK). The electrophoretic mobility of the particles was recorded from 12 cycles of 3 s each according to Smoluchowsky's model [25]. Measurements were performed at a concentration of 1 mg mL^{-1}. For all experiments, the ionic strength was kept constant by incorporating 200 mM $NaNO_3$ and adjusting the pH from 3 to 9 with HNO_3 and NaOH. Magnetic studies were carried out in a commercial superconducting quantum interferometer device (SQUID, Quantum Design, Inc., San Diego, CA, USA) at room temperature (T = 25 °C) for all samples, in the range of H = ±10,000 Oe. The magnetization was normalized to the saturation value of the particles (about 40 emu g^{-1} by Fe_3O_4@Oxa and 60–70 emu g^{-1} by Fe_3O_4, Fe_3O_4@Arg and Fe_3O_4@Cys). Infrared spectra were recorded with a Nicolet Magna 510 FT-IR spectrometer (Thermo Fisher Scientific, Waltham, MA, USA). The amounts of oxalate, arginine and cysteine loaded on the NPs were estimated by using thermogravimetric analysis in a simultaneous thermal analyzer, TA Instruments SDT Q600 (New Castle, DE, USA), in an atmosphere of N_2 (100 mL min^{-1}), the sample carrier was alumina pans, heating rate was 5 °C min^{-1}, and the final temperature was 800 °C. The structure and phase purity of the synthesized NPs were investigated by X-ray difractometry (XRD), using a powder X-ray diffractometer and a data acquisition program (Siemens diffractometer D5000, and DIFFRACplus, Munich, Germany). The filament was operated at 40 kV and 30 mA, emitting CuKα radiation of 0.154 nm. The NPs were ground in an agate mortar.

All measurements were made using slits of 2 mm, measuring an angular range between 20° and 70° with a step size of 0.02° and a step time of 1 s.

2.5. Bacteria Capture Experiments

P. putida strain was maintained in Petri dishes (4 °C) containing nutrient agar and replicated every 15 days. To start bacterial magnetic capture experiments, a colony of *P. putida* was inoculated into sterile tryptone soya broth (23 g L^{-1}, pH 5.0, Laboratorios Britania S.A., Buenos Aires, Argentina) and then grown aerobically on an orbital shaker at 32 °C. Cell growth was monitored with a spectrophotometer at 600 nm (OD_{600nm}) and colony forming units per mL (CFU mL^{-1}) were determined by dilution plating on Luria–Bertani (LB) agar medium after 24 h of cell growth at 32 °C (Figure S1). Cells were harvested until the early exponential phase was reached (OD_{600nm} = 1.0), then centrifuged at 14,000× *g* for 30 s and washed 2 times with citrate buffer (50 mM, pH 6). The bacterial concentration was adjusted to the desired level by measuring OD_{600nm}. In a typical capture experiment, 4 mg of NPs were suspended in 2 mL of citrate buffer saline (CBS, citric acid 50 mM, NaCl 136 mM and KCl 2.6 mM) and then agitated with a vortex. CBS was used for experiments at pHs 5 and 6, whereas phosphate buffer saline (PBS, phosphate 50 mM, NaCl 136 mM) was used when pH 7 or 8 was assayed. The required pH was adjusted with HCl or NaOH. The colloidal NPs suspension (with a given pH and buffer) was mixed with 2 mL of bacterial solution in a 15 mL Falcon tube (with the same pH and buffer) and then incubated for 30 min at 30 °C in an orbital shaker (200 rpm). As control experiments, plain CBS or PBS were mixed with the bacterial solution. After the incubation time, NPs were magnetically separated by using a magnet placed at the wall of the Falcon tube for a period of 10 min. Capture percentages were calculated as Equation (1) below:

$$\text{Capture (\%)} = (OD_0 - OD_f)\ 100/OD_0, \quad (1)$$

where OD_f is the OD_{600nm} value of the solution after the magnetic separation and OD_0 is the OD_{600nm} value of the control solution without magnetic NPs. We first investigated how NP concentration affects the bacteria capture efficiency by preparing a solution containing 0.1, 0.25, 0.5 and 1 mg L^{-1} of Fe_3O_4@Oxa, Fe_3O_4@Arg, Fe_3O_4@Cys and 5 × 10^7 UFC mL^{-1} of *P. putida* suspended in CBS 50 mM pH 5. On the other hand, we studied the range of bacteria suspensions that can be captured with the NPs synthesized. Finally, the effect of pH was examined with CBS (pH 5 and 6) and PBS (pH 7 and 8).

3. Results

3.1. Characterization of Fe_3O_4@Oxa, Fe_3O_4@Arg and Fe_3O_4@Cys

A typical FESEM micrograph of Fe_3O_4@Oxa, Fe_3O_4@Arg and Fe_3O_4@Cys, including the particle size distribution of each one is present in Figure 2. We obtained size distribution histograms after measuring at least 186 NPs by using Image J analysis software (version 1.51p, National Institutes of Health, Bethesda, MD, USA). The size of the magnetite NPs stabilized with oxalate was always close to 10 nm (details of each NPs can be observed in Figure 2), with a standard deviation (SD) of about 2 nm. The size and distribution of the NPs show minor changes with the two AAs used in this study. In this sense, the advantage of the synthesis procedure detailed in this article is to have the nucleation step separated from the functionalization one in order to control the NP size with the amount of oxalate and iron ions used.

The study results of EDS presented in Table 1 describes the composition of the NPs according to the functionalization made. As expected by the atomic composition of each compound, the NPs stabilized with amino acids show the presence of nitrogen. In the particular case of Fe_3O_4@Cys, the presence of S indicates that L-cysteine was present in the NPs.

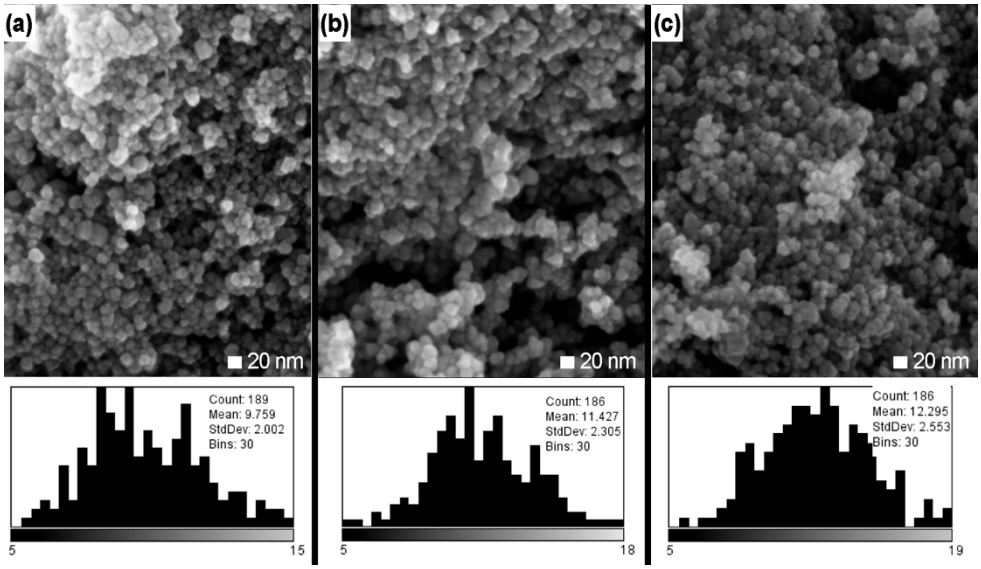

Figure 2. FE-SEM micrographs and size distribution analysis for all the prepared NPs. (**a**) Fe_3O_4@Oxa; (**b**) Fe_3O_4@Arg; and (**c**) Fe_3O_4@Cys. The scale bar (upper panels) represents 20 nm, as noted.

Table 1. Energy dispersive spectroscopy (EDS) analysis showing atomic percent present in the different nanoparticles (NPs).

NPs	C (%)	O (%)	Fe (%)	N (%)	S (%)
Fe_3O_4@Oxa	8.4	58.7	33.53	-	-
Fe_3O_4@Cys	30.54	39.6	11.09	8.61	10.16
Fe_3O_4@Arg	10.28	51.18	31.62	6.92	-

The zeta potential (Figure 3) of Fe_3O_4@Oxa ranged from 4 to −17.5 mV. Fe_3O_4@Cys show more positive values of zeta potential (23.9 to −19.3 mV), Fe_3O_4@Arg being even more positive (31.4 to −15.8 mV). These values were obtained in the total range of pH from 3 to 9 and under constant ionic strength ($NaNO_3$ 200 mM). For Fe_3O_4@Arg and Fe_3O_4@Cys, the zeta potential changed from positive to negative for a pH increment from 3 to 9 due to amine and acid group deprotonation.

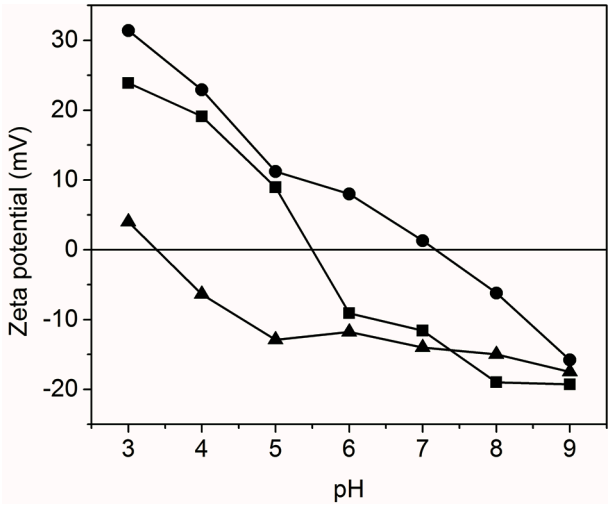

Figure 3. Zeta potential and pH relationship. Fe_3O_4@Oxa (triangle), Fe_3O_4@Arg (circle), and Fe_3O_4@Cys (square).

Figure 4 shows the magnetization curves of Fe_3O_4@Arg, Fe_3O_4@Cys and Fe_3O_4@Oxa. The curves described the superparamagnetic regime (reversible behavior) with zero coercive fields for all samples at room temperature.

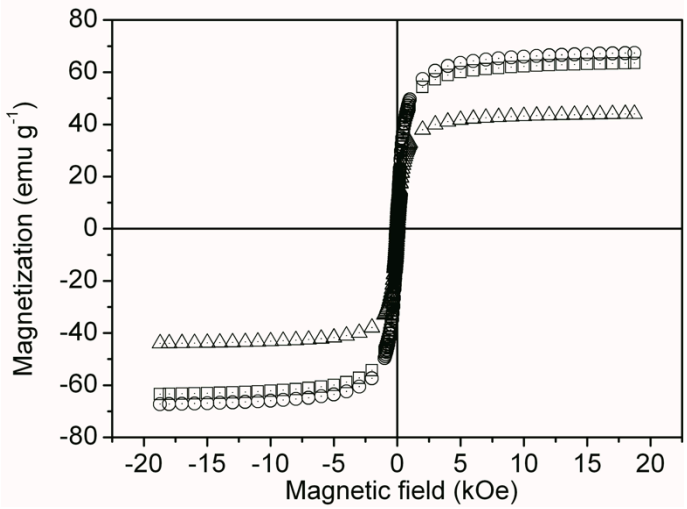

Figure 4. Magnetization curves at 25 °C. Fe_3O_4@Oxa (triangle), Fe_3O_4@Arg (circle), and Fe_3O_4@Cys (square).

We performed an FT-IR analysis in order to reveal the functional groups contained in the NPs after each synthesis step. It is well known that the presence of Fe_3O_4 is made evident by a stretching signal corresponding to metal–oxygen bond vibrations that commonly appear between 450 to 640 cm^{-1} [26]. In Figure 5b, it is possible to see stretching signals corresponding to Fe–O bonds vibrations at 581, 582 and 590 cm^{-1}. For all NPs synthetized in this study, we detected stretching signals corresponding to carboxyl group vibrations. In particular, C=O stretching and C–O–H in plane bending signals corresponding to the carboxylic acid can be observed at values closed to 1600 cm^{-1} and 1400 cm^{-1}, respectively [18,24,27]. We found a carbonyl signal at 1634 cm^{-1} for Fe_3O_4@Oxa, 1624 cm^{-1} for Fe_3O_4@Cys and 1653 cm^{-1} for Fe_3O_4@Arg; we also found C–O–H in plane bending signals at 1403 cm^{-1} for Fe_3O_4@Oxa, 1398 cm^{-1} for Fe_3O_4@Arg and 1408 cm^{-1} for Fe_3O_4@Cys. Peaks detected between 2500 and 3300 cm^{-1} correspond to O–H stretching signals of carboxylic acids. As can be seen in Figure 5a, both ammonium oxalate and Fe_3O_4@Oxa present strong O–H stretching signals when a molar ratio of Fe^{3+}:Fe^{2+}:$C_2O_4^{2-}$ equal to 2:1:1 was used in the first synthesis step, but when molar ratio was 2:1:0.1, as Tie et al. used [24], these signals did not appear (Figure S2). Taking into account these results, we decided to use ten times higher $C_2O_4^{2-}$ concentrations for the first synthesis step. In addition, in Figure 5a, we show that, in Fe_3O_4@Arg and Fe_3O_4@Cys spectra, O–H stretching signals are not strong, suggesting that oxalate is not present over the NPs. N–H signals corresponding to primary amines appear at 3400 cm^{-1} [24,28]. We detected the presence of amino acids on Fe_3O_4@Arg and Fe_3O_4@Cys NPs by the presence of N–H signals at 3409 and 3410 cm^{-1}, respectively. The lack of N–H stretching signals at the synthesis product of the first step (Fe_3O_4@Oxa) and the presence of the same signal after the second step (Fe_3O_4@Arg and Fe_3O_4@Cys) is in agreement with the synthesis procedure described in this study. In the case of pure cysteine (Figure 5a), the weak stretching signal at 2561 cm^{-1} belongs to S–H, which commonly appears near 2500 cm^{-1} [18]; however, these stretching signals were not present for Fe_3O_4@Cys. In the study of Schwaminger et al. [18], they show that cysteine absorbed to magnetite and can form S–S bonds between them, and this can be seen in the stretch between 500 and 530 cm^{-1} [29]. Figure 5b shows the presence of S–S signal at 539 cm^{-1}, suggesting that there is a molecular bond between two cysteine molecules over the surface of the NP. Moreover, the C–S stretching signal that commonly appears between 600 and 700 cm^{-1} was detected at 660 cm^{-1} for Fe_3O_4@Cys (Figure 5b).

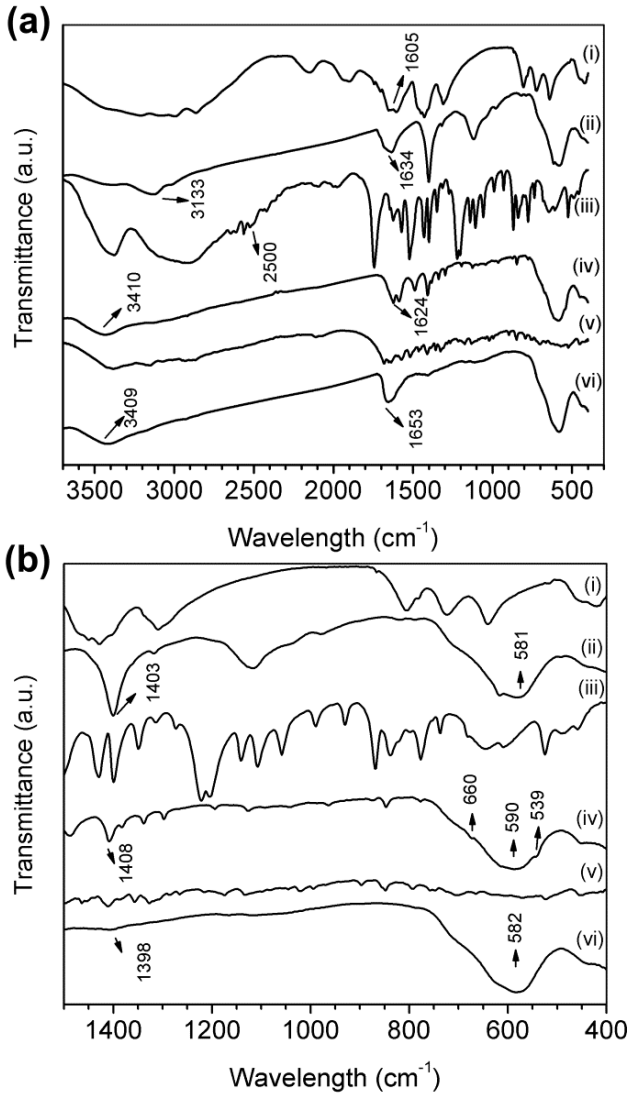

Figure 5. FT-IR spectra for the modified NPs and their modifiers. (**a**) shows the entire spectra and panel (**b**) shows the fingerprint range of (i) ammonium oxalate; (ii) Fe_3O_4@Oxa; (iii) L-cysteine; (iv) Fe_3O_4@Cys; (v) L-arginine and (vi) Fe_3O_4@Arg. The measurements were made at the spectral range between 4000 and 250 cm^{-1} with a resolution of 4 cm^{-1}.

The presence of the carboxylate and amino groups corresponding to the functionalization of the NPs with oxalate and the amino acids arginine and cysteine was demonstrated by FTIR spectroscopy and confirmed by thermogravimetric analysis (TGA). Two main weight loss steps were observed in the TGA curves of the samples Fe_3O_4@Oxa, Fe_3O_4@Arg and Fe_3O_4@Cys (Figure S3a). The first weight loss step observed in the temperature range from 30 to 200 °C was probably due to the loss of water in the samples [30]. The second weight loss step in the temperature region of 230–800 °C could be attributed to the decomposition of oxalate and the amino acids that wrap the NPs [24]. Our TGA trace for Fe3O4@Cys is similar to that obtained by other authors, when magnetic NP were synthesized using cysteine [24,31]. Thus, the TGA result confirms that the nanoparticles are coated with some amount of organic material. The weight loss at the end of the experiment (800 °C) was of 18.5, 10.5, and 16.5 for oxalate, cysteine and arginine, respectively. Considering that about 10% of the organic compounds remain as a residue at control samples (Figure S3b), the content of organics in NPs could be around 10% higher than the weight loss observed at Figure S3a.

Phase investigation of the crystallized product was performed by XRD and the diffraction pattern is presented in Figure S4. The XRD pattern indicates that the product mostly consists of magnetite Fe_3O_4, and the diffraction peaks are broadened owing to very small crystalline size. Observed diffraction peaks are indexed by the cubic structure of Fe_3O_4 (JCPDS No. 19-629), revealing a high phase purity of magnetite [24,32,33]. The line profile shown in Figure S4 was fitted for the observed seven peaks with the following miller indices: (111), (220), (311), (400), (422), (511) and (440) planes of a face-centered cubic (fcc) lattice of iron oxide. The corresponding lattice constant is t = 10.699 nm. The functionalization with arginine or cysteine does not alter the crystalline structure of magnetite.

3.2. Bacteria Capture Experiments

The efficiency of magnetic capture was performed with different concentrations of the three NPs synthesized. It is well known that many bacteria species have a negative net charge over the external membrane surface; therefore, positive charged NPs can be attracted to bacteria by electrostatic interactions [21,22,34]. This has been the main criteria to choose capture NP systems. However, some other forces can be relevant, as will be discussed in the next section. All three NP systems studied here could be separated from the bulk solution with the aid of a magnet in less than 5 min and the same behavior was appreciated when preliminary bacteria capture experiments were done (data not shown). Taking these into account, during the magnetic capture procedure, we used 10 min in order to avoid time-related experimental error.

NP concentrations greater than 1 mg mL^{-1} were avoided due to the instability of the suspension in time (t > 30 min). Agglomeration and clumping of relatively concentrated magnetic NP are well known and reported in previously published work [35].

As can be seen in Figure 6, there is a direct relationship between the NP concentration used and the capture efficiency; furthermore, there is a similar behavior for both AA-modified NPs used. In all cases, we used 5 × 10^7 CFU mL^{-1} of *P. putida* suspended in citrate buffer saline (50 mM, pH 6). NP concentrations greater than 1 mg mL^{-1} were avoided due to the instability of the suspension in time (t > 30 min). For the subsequent experiments, a concentration of 1 mg mL^{-1} of NPs was selected since, in these conditions, a higher capture efficiency was achieved.

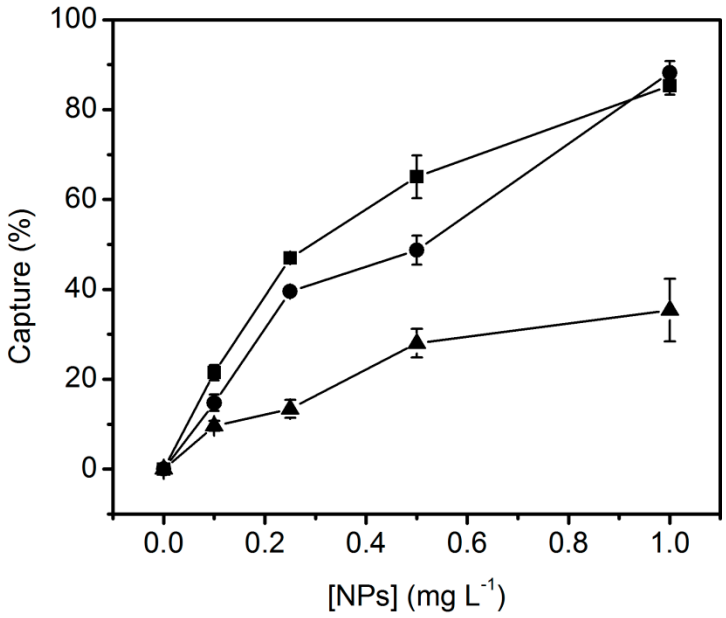

Figure 6. Capture efficiency and NP concentration relationship. Experiments were performed in citrate buffer saline (CBS) 50 mM (pH 5.0) with 5 × 10^7 colony forming units (CFU) mL^{-1} of *P. putida* using Fe_3O_4@Oxa (triangle), Fe_3O_4@Arg (circle) or Fe_3O_4@Cys (square).

Figure 7 shows the relationship between capture efficiency and microorganism's concentration. For microorganism's concentrations above 1×10^8 CFU mL^{-1}, a significant decrease in the capture efficiency can be observed.

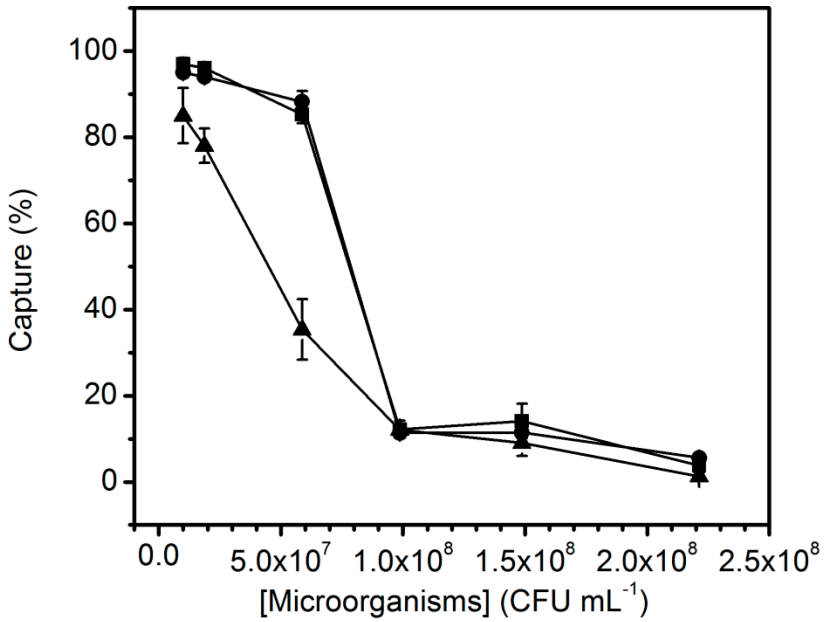

Figure 7. Capture efficiency and microorganisms' concentration relationship. Experiments were performed with *P. putida* suspended in CBS (pH 5) using 1 mg mL^{-1} of Fe_3O_4@Oxa (triangle), Fe_3O_4@Arg (circle) or Fe_3O_4@Cys (square).

4. Discussion

In this work, we have obtained superparamagnetic Fe_3O_4 NPs stabilized with AAs in a single functionalization step, using a process involving chemical co-precipitation with ferrous/ferric precursors and oxalate anion in the first step followed by a substitution at the second step. With changes in the synthesis, and followed by a simple but effective washing procedure between steps, we achieved a superparamagnetic NPs system with more uniform size than that proposed by Tie et al. [24] as well as high reproducibility. All systems showed a similar average particle size of ca. 10 nm. Moreover, EDS studies show confirmatory information about the successful modification of the NPs with oxalate, arginine or cysteine, as the atomic composition was the expected for each one.

The isoelectric point of Fe_3O_4@Oxa was 3.4, which is related to the equilibrium constant for the loss of the first and the second proton of oxalate (pK_a = 1.27 and 4.28). For Fe_3O_4@Arg and Fe_3O_4@Cys, the isoelectric points were 7.2 and 5.5, respectively. These results are the expected with the well-known structure and amine groups in the amino acids used, and so, with the bibliographic values of isoelectric point of L-arginine and L-cysteine, are 11.5 and 5.02, respectively.

The negative values of zeta potential on the surface stabilized oxalate NPs, throughout the pH range was produced by the high affinity that carboxyl groups presented in the magnetite [36], which undergo a sudden change when they were functionalized with amino acids. This change provides to the surface of the NP systems a positive charge at acidic pH values and negative values at basic pH, giving to the surface of the NPs a wider range of load charge, at constant ionic strength and at broad pH range, which has been demonstrated by zeta potential measurements.

The magnetization curves of all NP systems (Fe_3O_4@Arg, Fe_3O_4@Cys, and Fe_3O_4@Oxa) showed no hysteresis, producing a superparamagnetic behavior at room temperature. The primary particle size obtained in our work is in good agreement with the superparamagnetic limit of magnetite NPs, which is below 20 nm. It can be seen that the magnetization of Fe_3O_4@Oxa is 44.03 emu g^{-1} (Figure 4),

and this value is smaller than those reported by Tie et al. [24]. The lower magnetization could be related to a higher ligand density over the NP surface taking into account that we use ten times higher concentration of $C_2O_4^{2-}$ in the first step in comparison with Tie et al. [24]. This is in agreement with the fact that if ligand density increases, the magnetization decreases. Amino acid coated NPs have a higher saturation of magnetization than oxalate stabilized ones, being 66.41 emu g^{-1} and 62.05 emu g^{-1} for Fe_3O_4@Arg and Fe_3O_4@Cys, respectively. Yan's group [33] has produced AAs coated Fe_3O_4 NPs for bacterial capture applications, but, due to the silica shell used in the first step of the synthesis procedure, they obtained a low saturation of magnetization (12 emu g^{-1}). The saturation of magnetization values obtained in this study is in the typical range obtained by other authors, who used them for bacterial capture [21] and other applications [27].

An interesting feature observed in Figure 4 is that when NPs wrapped with a small molecule (as oxalate) are replaced by bigger ones (as the amino acids), magnetization increases, although a magnetization decrease was expected (same magnetic core, more non-magnetic organic wrap). Previous work shows that magnetic properties of NPs are strongly determined by NP size, where saturation magnetization increases with increasing crystal size until a size of 12 nm [37]. Magnetization measurements provide a weighted average of all the NPs dispersed in the solution. We believe the higher NP size and magnetization of the amino acid-modified particles is related to the washing procedure, which involves a magnetic separation step that can select the bigger and more magnetic NPs, against the smaller ones, as can be seen in Figure 2.

We were able to identify the signals obtained by FT-IR corresponding to functional groups for both pure compounds and the synthetized NPs. The FTIR spectra in Figure 5 shows the presence of Fe–O interaction and the carbon chains of both the oxalate and the amino acids used, which cover the three NPs synthesized here. OH– and COOH groups are shown in both the oxalate and in the Fe_3O_4@Oxa system, as expected. Moreover, $–NH_2$ groups are evident the amino acids functionalized nanoparticles (Fe_3O_4@Arg and Fe_3O_4@Cys).

Furthermore, if we make a comparison between the FT-IR spectra of pure AAs and the respective Fe_3O_4@AAs in the fingerprint region (1500–400 cm^{-1}), we can appreciate that there is a remarkable correlation between the curves, suggesting that we successfully cover the NPs with the AAs. In this study, we considered having a successful AA functionalization by the presence of at least three FT-IR signals corresponding to N–H near 3400 cm^{-1}, C=O at 1600 cm^{-1} and C–O–H at 1400 cm^{-1}. A significant change in the zeta potential curve of the NPs after being stabilized with AAs shows that the second step of the synthesis was successfully done, in concordance with all the other data present here. This includes FT-IR, and the elemental analysis of each type of NP, showing the presence of carbon-containing functional groups at all NPs, nitrogen-containing functional groups only on the amino acid modified ones, and sulfur-containing functional groups only when we use the sulfur containing AA, as expected.

Capture efficiency in terms of absolute CFU mg^{-1} of NPs achieved in our work is higher than those values reported in literature (Table 2), taking into account similar NP size for the comparison. Other studies have been shown to capture 4.9×10^7 CFU mg^{-1} of NPs by using microparticles of 150 nm [38]. Besides the better capture efficiency, in comparison with our study, Chen et al. [38] Fe_3O_4 particles were functionalized with mesoporus silica and cetyltrimethylammonium bromide (CTAB), which are not conventional reagents for a low-cost application; in addition, they showed low saturation magnetization (50 emu g^{-1}). The NPs presented in this study can capture at least 3×10^7 CFU mL^{-1} when 1 mg mL^{-1} of Fe_3O_4@Arg or Fe_3O_4@Cys is used. Moreover, we studied the capture efficiency under different pH conditions (5–8), and all AA-modified NPs seem to capture more than 3×10^7 CFU mL^{-1}, as it can be appreciated in Figure 8.

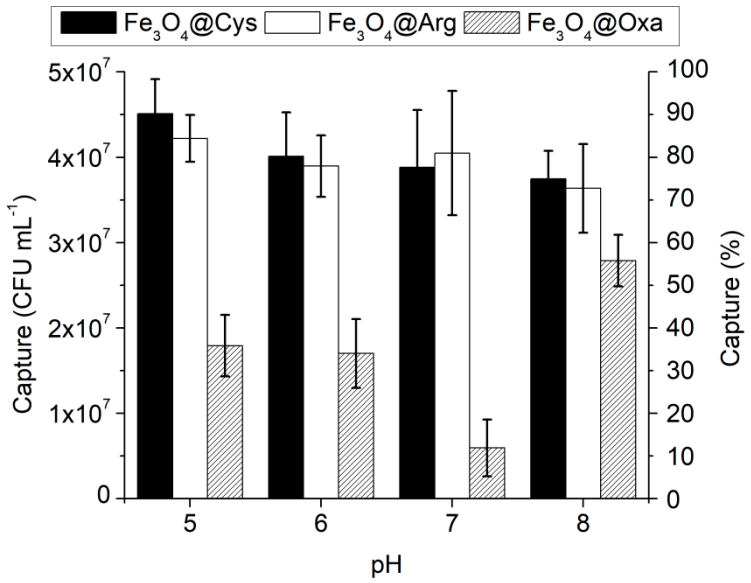

Figure 8. Capture efficiency and pH relationship. Experiments were performed in CBS 50 mM (pH 5) and phosphate buffer saline (PBS) 50 mM (pH 6, 7 and 8. NPs and bacterial concentration used were 1 mg mL^{-1} and 5 × 10^7 CFU mL^{-1}, respectively. Fe_3O_4@Arg (black bars), Fe_3O_4@Cys (white bars) and Fe_3O_4@Oxa (pattern bars).

Table 2. Comparison of the synthesized NPs used for bacteria capture with other published results.

NPs	Size (nm)	Capture Media (pH)	V (mL)	NPs (mg mL^{-1})	CFU mL^{-1} before Incubation	Incubation (min)	Capture Efficiency (%)	Ref.
Fe_3O_4@Oxa	9.8 ± 2.0	CBS (5)	2	1	1 × 10^7 (*P. putida*)	30	85	This work
Fe_3O_4@Arg	11.4 ± 2.3	CBS (5)	2	1	1 × 10^7 (*P. putida*)	30	95	This work
Fe_3O_4@Cys	12.3 ± 2.5	CBS (5)	2	1	1 × 10^7 (*P. putida*)	30	97	This work
Fe_3O_4@mSiO_2/CTAB	150	PBS (*ns*)	2	0.2	≈10^7 (*B. subtillis* or *E. coli*)	10	98	[38]
Fe_3O_4@Arg	10	H_2O (6)	5	0.8	1.5 × 10^7 (*E. coli*)	30	97	[21]
Fe_3O_4@Man	10	PBS (*ns*)	1	2	1.5 × 10^6 (*E. coli*)	45	83.5	[39]
Fe_3O_4@AF	*ns*	PBS (7)	5	1	*ns*, OD_{600nm} = 1 (*E. coli*)	1	97	[33]

Arg, arginine. CBS, citrate buffer saline. Cys, cysteine. CTAB, cetyltrimethylammonium bromide. PBS, phosphate buffer saline. Man, D-mannose. AF, amine functionalized. *ns*, not specified in the original work.

Surface charge of bacteria and NPs had been previously considered as the main force of interaction between them by means of strong electrostatic attractions [40]. Other authors have shown [21,33] that there is not a strict correlation between the capture efficiency and the pH when Fe_3O_4@AAs NPs were used, indicating that the electrostatic forces are not the only forces involved in the binding process. Moreover, hydrophobic forces could be dominating the Fe_3O_4@AAs adhesion to cell membranes [21,41]. In addition, bacteria capture experiments in a pH range from 2 to 11 [33] and from 4 to 10 [21] were performed, showing that the amino functionalized magnetic nanoparticles can capture *E. coli* independently from the acidity of the solution. In a recent work, gold NPs modified with the dipeptide L-alanyl-L-alanine negative charged show strong interactions with identically charged Gram-negative and -positive bacteria, interactions that are not fully explained in this work [42]; alanine is classified as an hydrophobic amino acid and this force could be relevant in the NP-bacteria interactions.

Here, we synthesized Fe_3O_4@AAs, which shows a high efficiency for the magnetic capture of bacteria when assayed in different buffers and pHs; Fe_3O_4@Oxa, as expected, was less efficient. When the three NPs were assayed at pH 6 (where Fe_3O_4@Oxa and Fe_3O_4@Cys have a negative charge, but Fe_3O_4@Arg has a positive charge), our results show that electrostatic forces are not the more relevant aspect to be considered when bacterial–NP interactions are considered. A property that shares both Fe_3O_4@AAs is their hydrophobic character, in which they differ from Fe_3O_4@Oxa NPs. The most hydrophobic NPs is Fe_3O_4@Cys, being followed by Fe_3O_4@Arg and lastly Fe_3O_4@Oxa, so this type of interaction seems to be the most relevant to explain the interactions between bacteria and NPs; a simple contact angle experiment shows that Fe_3O_4@Arg and Fe_3O_4@Cys are more hydrophobic than Fe_3O_4@Oxa. Details and results are included in Supplementary Materials, Figure S5.

5. Conclusions

Hydrophobic and electrostatic forces are proposed to be the key factors affecting the bacterial attachment to different material surfaces, the mechanisms governing these phenomena not being clear. We conclude that amino acid nature is not relevant when interactions with the model bacteria we used here are considered, and that unspecific processes such as hydrophobic interactions must be the prevalent forces implicated in the capture process among others. The hydrophobicity of the bacterial cell wall allows them to interact with other cells or surfaces with similar hydrophobicity [43]. There are a high number of studies that show that increasing the hydrophobicity of bacterial surfaces or substrate surfaces produce an enhanced number of cells attached [44,45]. Recent studies show that Gram-negative bacteria tend to interact mostly with hydrophobic materials as graphene oxide [46,47] or magnetic NPs stabilized with hydrophobic ligands in comparison with hydrophilic ligands [48].

Hydrophobic interaction between NPs and the extracellular polymeric substances (EPS), lipopolysaccharides, and hydrophobic residues of membrane proteins and lipoproteins seems to be relevant [49], given that the capture efficiency remains similar when pH, and thus bacterial and NP charge were affected. The importance of hydrophobic forces in peptide–protein interactions have been reviewed [50], and the principles can be extended to the amino acid residues wrapping the NPs synthesized here and proteins present in the outer bacterial wall and membrane. Our findings give new and relevant insights when the synthesis of effective nanoparticulate systems, designed to capture microbial cells, is the goal.

Supplementary Materials: The Supplementary Materials are available online at http://www.mdpi.com/2504-5377/2/3/29/s1.

Author Contributions: Conceptualization, F.F., A.S., E.C. and V.E.D.; Methodology, F.F., A.S. and V.E.D.; Validation, E.C., F.F., A.S. and V.E.D.; Formal Analysis, V.E.D., E.C., A.S., and F.F.; Investigation, F.F. and A.S.; Resources, E.C. and V.E.D.; Data Curation, F.F.; Writing—Original Draft Preparation, F.F. and A.S.; Writing-Review and Editing, F.F., E.C. and V.E.D.; Supervision, E.C.; Project Administration, E.C. and V.E.D.; Funding Acquisition, E.C.

Funding: The work presented here was funded by the National Agency of Scientific and Technological Promotion (ANPCyT), by the grants 'BID-PICT 2013-0033' and 'BID-PICT 2014-0402'. The authors also appreciate the grant provided by the CONICET, award No. PIP 2015 2017 GI. All of the grants were received by the author E.C.

Acknowledgments: We also want to thank to Lic. Silvia Rodriguez and Sebastian Cortón for editing our manuscript.

Conflicts of Interest: The authors declare no conflict of interest.

References

1. Roger, J.; Pons, J.N.; Massart, R.; Halbreich, A.; Bacri, J.C. Some biomedical applications of ferrofluids. *Eur. Phys. J. Appl. Phys.* **1999**, *5*, 321–325. [CrossRef]
2. Sun, S.; Murray, C.B.; Weller, D.; Folks, L.; Moser, A. Monodisperse FePt nanoparticles and ferromagnetic FePt nanocrystal superlattices. *Science* **2000**, *287*, 1989–1992. [CrossRef] [PubMed]

3. Miller, M.M.; Prinz, G.A.; Cheng, S.F.; Bounnak, S. Detection of a micron-sized magnetic sphere using a ring-shaped anisotropic magnetoresistance-based sensor: A model for a magnetoresistance-based biosensor. *Appl. Phys. Lett.* **2002**, *81*, 2211–2213. [CrossRef]
4. Chourpa, I.; Douziech-Eyrolles, I.; Ngaboni-Okassa, L.; Fouquenet, J.F.; Cohen-Jonathan, S.; Soucé, M.; Marchis, H.; Dubois, P. Molecular composition of iron oxide nanoparticles, precursors for magnetic drug targeting, as characterized by confocal Raman microspectroscopy. *Analyst* **2005**, *130*, 1395–1403. [CrossRef] [PubMed]
5. Boutry, S.; Laurent, S.; Elst, L.V.; Muller, R.N. Specific E-selectin targeting with a superparamagnetic MRI contrast agent. *Contrast Media Mol. Imaging* **2006**, *1*, 15–22. [CrossRef] [PubMed]
6. Corot, C.; Robert, P.; Idée, J.M.; Port, M. Recent advances in iron oxide nanocrystal technology for medical imaging. *Adv. Drug Deliv. Rev.* **2006**, *58*, 1471–1504. [CrossRef] [PubMed]
7. Sambucetti, C. Magnetic ink for jet printing. *IEEE Trans. Med. Imaging* **1980**, *16*, 364–367. [CrossRef]
8. Gupta, A.K.; Wells, S. Surface-modified superparamagnetic nanoparticles for drug delivery: Preparation, characterization, and cytotoxicity studies. *IEEE Trans. Nanotechnol.* **2004**, *3*, 66–73. [CrossRef]
9. Kim, D.K.; Zhang, Y.; Voit, W.; Rao, K.V.; Muhammed, M.J. Synthesis and characterization of surfactant-coated superparamagnetic monodispersed iron oxide nanoparticles. *J. Magn. Magn. Mater.* **2001**, *225*, 30–36. [CrossRef]
10. Jolivet, J.P. *Metal Oxide Chemistry and Synthesis: From Solution to Solid State*; Wiley and Sons Ltd.: West Sussex, UK, 2000.
11. Vayssières, L.; Chanéac, C.; Tronc, E.; Jolivet, J.P. Size tailoring of magnetite particles formed by aqueous precipitation: An example of thermodynamic stability of nanometric oxide particles. *J. Colloid Interface Sci.* **1998**, *205*, 205–212. [CrossRef] [PubMed]
12. Tartaj, P.; Morales, M.P.; Veintemilla-Verdaguer, S.; Gonzalez-Carreno, T.; Serna, C.J. Synthesis, properties and biomedical applications of magnetic nanoparticles. In *Handbook of Magnetic Materials*; Buschow, K.H.J., Ed.; Elsevier: Amsterdam, The Neverthelands, 2006; Volume 16, pp. 403–482.
13. Dunlop, D.J.; Özdemir, Ö. *Rock Magnetism: Fundamentals and Frontiers*; Cambridge University Press: Cambridge, UK, 1997.
14. Vincent, B.; Edwards, J.; Emment, S.; Jones, A. Depletion flocculation in dispersions of sterically-stabilised particles ('soft spheres'). *Colloids Surf.* **1986**, *18*, 261–281. [CrossRef]
15. Laurent, S.; Forge, D.; Port, M.; Roch, A.; Robic, C.; Vander Elst, L.; Muller, R.N. Magnetic iron oxide nanoparticles: Synthesis, stabilization, vectorization, physicochemical characterizations, and biological applications. *Chem. Rev.* **2008**, *108*, 2064–2110. [CrossRef] [PubMed]
16. Cornell, R.M.; Schwetmann, U. *The Iron Oxides: Structure, Properties, Reactions, Occurrences and Uses*, 2nd ed.; Wiley-VCH: Weinheim, Germany, 2006.
17. Massart, R.; Dubois, E.; Cabuil, V.; Hasmonay, E. Preparation and properties of monodisperse magnetic fluids. *J. Magn. Magn. Mater.* **1995**, *149*, 1–5. [CrossRef]
18. Schwaminger, S.P.; García, P.F.; Merck, G.K.; Bodensteiner, F.A.; Heissler, S.; Günther, S.; Berensmeier, S. Nature of interactions of amino acids with bare magnetite nanoparticles. *J. Phys. Chem. C* **2015**, *119*, 23032–23041. [CrossRef]
19. Koo, H.; Allan, R.N.; Howlin, R.P.; Hall-Stoodley, L.; Stoodley, P. Targeting microbial biofilms: Current and prospective therapeutic strategies. *Nat. Rev. Microbiol.* **2017**, *15*, 740–755. [CrossRef] [PubMed]
20. Kumar, M.; Curtis, A.; Hoskins, C. Application of nanoparticle technologies in the combat against anti-microbial resistance. *Pharmaceutics* **2018**, *10*, 11. [CrossRef] [PubMed]
21. Jin, Y.; Liu, F.; Shan, C.; Tong, M.; Hou, Y. Efficient bacterial capture with amino acid modified magnetic nanoparticles. *Water Res.* **2014**, *50*, 124–134. [CrossRef] [PubMed]
22. Abenojar, E.C.; Wickramasinghe, S.; Ju, M.; Uppaluri, S.; Klika, A.; George, J.; Barsoum, W.; Frangiamore, S.J.; Higuera-Rueda, C.A.; Samia, A.C.S. Magnetic glycol chitin-based hydrogel nanocomposite for combined thermal and D-amino-acid-assisted biofilm disruption. *ACS Infect. Dis.* **2018**, *10*, 11. [CrossRef] [PubMed]
23. Kallay, N.; Matijevic, E. Adsorption at solid/solution interfaces. 1. Interpretation of surface complexation of oxalic and citric acids with hematite. *Langmuir* **1985**, *1*, 195–201. [CrossRef]
24. Tie, S.L.; Lin, Y.Q.; Lee, H.C.; Bae, Y.S.; Lee, C.H. Amino acid-coated nano-sized magnetite particles prepared by two-step transformation. *Colloids Surf. A* **2006**, *273*, 75–83. [CrossRef]

25. Cametti, C.; Codastefano, P.; Tartaglia, P. Aggregation kinetics in model colloidal systems: A light scattering study. *J. Colloid Interface Sci.* **1989**, *131*, 409–422. [CrossRef]
26. Bromberg, L.; Chang, E.P.; Hatton, T.A.; Concheiro, A.; Magariños, B.; Alvarez-Lorenzo, C. Bactericidal core-shell paramagnetic nanoparticles functionalized with poly(hexamethylene biguanide). *Langmuir* **2011**, *27*, 420–429. [CrossRef] [PubMed]
27. Vieira, A.P.; Berndt, G.; de Souza, I.G., Jr.; Di Mauro, E.; Paesano, A., Jr.; de Santana, H. Adsorption of cysteine on hematite, magnetite and ferrihydrite: FT-IR, Mössbauer, EPR spectroscopy and X-ray diffractometry studies. *Amino Acids* **2011**, *40*, 205–214. [CrossRef] [PubMed]
28. Ünal, B.; Durmus, Z.; Baykal, A.; Sözeri, H.; Toprak, M.S.; Alpsoy, L. L-Histidine coated iron oxide nanoparticles: Synthesis, structural and conductivity characterization. *J. Alloys Compd.* **2010**, *505*, 172–178. [CrossRef]
29. Bastian, E.J.; Martin, R.B. Disulfide vibrational spectra in the sulfur-sulfur and carbon-sulfur stretching region. *J. Phys. Chem.* **1973**, *77*, 1129–1133. [CrossRef]
30. La, B.H.; Yeh, C.C.; Chen, D.H. Surface modification of iron oxide nanoparticles with polyarginine as a highly positively charged magnetic nano-adsorbent for fast and effective recovery of acid proteins. *Process. Biochem.* **2012**, *47*, 799–805. [CrossRef]
31. Sangeetha, J.; Philip, J. Synthesis, characterization and antimicrobial property of Fe_3O_4-Cys-HNQ nanocomplex, with L-cysteine molecule as a linker. *RSC Adv.* **2013**, *3*, 8047–8057. [CrossRef]
32. Wejrzanowski, T.; Pielaszek, R.; Opalinska, A.; Matysiak, H.; Lojkowski, W.; Kurzydlowski, K.J. Quantitative methods for nanopowders characterization. *Appl. Surf. Sci.* **2006**, *253*, 204–208. [CrossRef]
33. Huang, Y.F.; Wang, Y.F.; Yan, X.P. Amine-functionalized magnetic nanoparticles for rapid capture and removal of bacterial pathogens. *Environ. Sci. Technol.* **2010**, *44*, 7908–7913. [CrossRef] [PubMed]
34. Honda, H.; Kawabe, A.; Shinkai, M.; Kobayashi, T. Development of chitosan-conjugated magnetite for magnetic cell separation. *J. Ferment. Bioeng.* **1998**, *86*, 191–196. [CrossRef]
35. Xu, Z.Z.; Wang, C.C.; Yang, W.L.; Deng, Y.H.; Fu, S.K. Encapsulation of nanosized magnetic iron oxide by polyacrylamide via inverse miniemulsion polymerization. *J. Magn. Magn. Mater.* **2004**, *277*, 136–143. [CrossRef]
36. Angermann, A.; Töpfer, J. Synthesis of magnetite nanoparticles by thermal decomposition of ferrous oxalate dihydrate. *J. Mater. Sci.* **2008**, *43*, 5123–5130. [CrossRef]
37. Smolensky, E.D.; Park, H.Y.; Zhou, Y.; Rolla, G.A.; Marjańska, M.; Botta, M.; Pierre, V.C. Scaling laws at the nano size: The effect of particle size and shape on the magnetism and relaxivity of iron oxide nanoparticle contrast agents. *J. Mater. Chem. B* **2013**, *1*, 2818–2828. [CrossRef] [PubMed]
38. Chen, G.; Li, Z.; Wang, X.; Xie, L.; Qi, Q.; Fang, W. Preparation of CTAB-loaded magnetic nanospheres for rapid bacterial capture and decontamination. *Mater. Lett.* **2014**, *134*, 290–294. [CrossRef]
39. El-Boubbou, K.; Gruden, C.; Huang, X. Magnetic glyco-nanoparticles: A unique tool for rapid pathogen detection, decontamination, and strain differentiation. *J. Am. Chem. Soc.* **2007**, *129*, 13392–13393. [CrossRef] [PubMed]
40. Ranmadugala, D.; Ebrahiminezhad, A.; Manley-Harris, M.; Ghasemi, Y.; Berenjian, A. Magnetic immobilization of bacteria using iron oxide nanoparticles. *Biotechnol. Lett.* **2018**, *40*, 237–248. [CrossRef] [PubMed]
41. Van Loosdrecht, M.C.; Lyklema, J.; Norde, W.; Schraa, G.; Zehnder, A.J. Electrophoretic mobility and hydrophobicity as a measured to predict the initial steps of bacterial adhesion. *Appl. Environ. Microb.* **1987**, *53*, 1898–1901.
42. Yang, X.; Dang, Y.; Lou, J.; Shao, H.; Jiang, X. D-alanyl-D-alanine-modified gold nanoparticles form a broad-spectrum sensor for bacteria. *Theranostics* **2018**, *8*, 1449–1457. [CrossRef] [PubMed]
43. Geoghegan, M.; Andrews, J.S.; Biggs, C.A.; Eboigbodin, K.E.; Elliott, D.R.; Rolfe, S.; Scholes, J.; Ojeda, J.J. The polymer physics and chemistry of microbial cell attachment and adhesion. *Faraday Discuss.* **2008**, *139*, 85–103. [CrossRef] [PubMed]
44. Yousefi Rad, A.; Ayhan, H.; Pişkin, E. Adhesion of different bacterial strains to low-temperature plasma-treated sutures. *J. Biomed. Mater. Res.* **1998**, *41*, 349–358. [CrossRef]
45. Roosjen, A.; Busscher, H.J.; Norde, W.H.; van der Mei, C. Bacterial factors influencing adhesion of *Pseudomonas aeruginosa* strains to a poly(ethylene oxide) brush. *Microbiology* **2006**, *152*, 2673–2682. [CrossRef] [PubMed]

46. Xue, J.; BinAhmed, S.; Wang, Z.; Karp, N.G.; Stottrup, B.L.; Romero-Vargas Castrillón, S. Bacterial adhesion to graphene oxide (GO)-functionalized interfaces is determined by hydrophobicity and GO sheet spatial orientation. *Environ. Sci. Technol. Lett.* **2017**, *5*, 14–19. [CrossRef]
47. Zhan, S.; Zhu, D.; Ma, S.; Yu, W.; Jia, Y.; Li, Y. Highly efficient removal of pathogenic bacteria with magnetic graphene composite. *ACS Appl. Mater. Interfaces* **2015**, *7*, 4290–4298. [CrossRef] [PubMed]
48. Huang, X.; Xiong, Y.; Lu, L.; Liu, J.; Peng, K. Manipulation of surface hydrophobicity and charge of demulsifying bacteria using functional magnetic nanoparticles: A mechanistic study of demulsification performance. *Energy Fuels* **2017**, *31*, 3295–3304. [CrossRef]
49. Darabdhara, G.; Boruah, P.K.; Hussain, N.; Borthakur, P.; Sharma, B.; Sengupta, P.; Das, M.R. Magnetic nanoparticles towards efficient adsorption of Gram positive and Gram negative bacteria: An investigation of adsorption parameters and interaction mechanism. *Colloids Surf. A Physicochem. Eng. Asp.* **2017**, *516*, 161–170. [CrossRef]
50. Cserháti, T.; Szögyi, M. Role of hydrophobic and hydrophilic forces in peptide-protein interaction: New advances. *Peptides* **1995**, *16*, 165–173. [CrossRef]